ELSEVIER

Journal of Alloys and Compounds 356–357 (2003) 497–500

Journal of ALLOYS AND COMPOUNDS

www.elsevier.com/locate/jallcom

Characterization of Ti–Zr–Mn–V-based Laves phase alloys for MH refrigeration system

Y. Shudo*, T. Ebisawa, H. Itoh

Muroran Research Laboratory, The Japan Steel Works, 4 Chatsu-machi, Muroran, Hokkaido 051-8505, Japan

Received 1 September 2002; received in revised form 6 December 2002; accepted 6 February 2003

Abstract

Ti–Zr–Mn–V based C14 Laves phase alloys have been developed, aiming for application to the metal hydride (MH) refrigeration system, because of their large hydrogen storage capacities and good plateau properties. The melt-spinning process, which was applied to the manufacturing of some of these alloys, could make the plateau slopes much flatter. In the present work, observations of the microstructures were carried out with regard to both Ti–Zr–Mn–V–Fe and Ti–Mn–V–Fe alloys, which are practical compounds for use in the MH refrigeration system. It was revealed that the segregation of zirconium in the $Ti_{23}Zr_{10}Mn_{46.5}V_{17}Fe_{3.5}$ alloy and the precipitation of $E9_3$ structure oxide phase in the $Ti_{35}Mn_{47}V_{15}Fe_3$ alloy affected their plateau properties. It appears that, in order to improve the plateau property of these alloys, compositional homogenization and lowering of the oxygen are desirable.

Keywords: Hydrogen storage; Laves phase alloy; Microstructure; Refrigeration system

1. Introduction

Ti–Mn based C14 type Laves phase alloys have attracted attention as hydrogen storage materials, because of their large storage capacities, easy activation and fast hydriding–dehydriding kinetics [1]. In particular, Ti–Zr–Mn–V-based alloy systems have been developed for application to the metal hydride (MH) refrigeration system utilizing waste heat, because a favorable hydrogen pressure could be obtained for altering the compositional ratio between titanium and zirconium [2] and the plateau slopes were comparatively flatter [3]. Furthermore, it was revealed that applying the melt-spinning process to the manufacturing of the $Ti_{23}Zr_{10}Mn_{50}V_{17}$ alloy, which was used for waste heat utilization, could make the plateau slopes flatter, resulting in an increase in the effective transfer capacities of hydrogen [4]. However, regarding the melt-spun $Ti_{35}Mn_{50}V_{15}$ alloy, which was used for refrigeration output, the plateau slopes did not become flatter and it was supposed that Ti-rich precipitates in this alloy influenced the hydrogen storage properties [4]. In the present work, observations of the microstructures were carried out on both Ti–Zr–Mn–V–Fe and Ti–Mn–V–Fe alloys, which are practical compounds for using the MH refrigeration system, in order to clarify the relationship between the microstructure and hydriding properties.

2. Experimental

The starting materials were titanium (99 wt.%), zirconium (99 wt.%), manganese (99.9 wt.%) and ferrovanadium (containing about 85 wt.% vanadium, 15 wt.% iron and inevitable impurities, aluminum, silicon, and so on). The $Ti_{23}Zr_{10}Mn_{46.5}V_{17}Fe_{3.5}$ and $Ti_{35}Mn_{47}V_{15}Fe_3$ experimental alloys were prepared by argon arc melting. The obtained ingots were used for annealing at 1373 K for 24 h or for melt-spinning onto a copper roll. Pressure–composition (P–C) isotherms were measured in a conventional Sieverts-type apparatus. The $Ti_{23}Zr_{10}Mn_{46.5}V_{17}Fe_{3.5}$ alloy samples were sufficiently degassed at 433 K before each treatment. Initial hydrogenation was carried out at 293 K under a hydrogen pressure of 4 MPa. In the case of the $Ti_{35}Mn_{47}V_{15}Fe_3$ alloy, degasification at 353 K and initial hydrogenation at 253 K under hydrogen pressure of 4 MPa

*Corresponding author.
E-mail address: yk_shudo@ceri.go.jp (Y. Shudo).

0925-8388/03/$ – see front matter
doi:10.1016/S0925-8388(03)00365-7

were carried out. Furthermore, X-ray powder diffraction (XRD) analysis by using CuKα radiation was carried out to determine phases and lattice constants. The microstructure of these alloys was observed and analyzed by scanning electron microscopy (SEM), electrons probe X-ray microanalysis (EPMA), transmission electron microscopy (TEM) and energy dispersive X-ray spectroscopy (EDS).

3. Results and discussion

3.1. $Ti_{23}Zr_{10}Mn_{46.5}V_{17}Fe_{3.5}$ alloy

The *P–C* isotherms of the $Ti_{23}Zr_{10}Mn_{46.5}V_{17}Fe_{3.5}$ alloy, which were used for waste heat utilization, are shown in Fig. 1. After annealing, the *P–C* isotherms had sloping plateaus and the plateau property did not improve significantly. In contrast, after melt-spinning, the plateau slopes were much flatter than those of the annealed sample. The XRD patterns of the $Ti_{23}Zr_{10}Mn_{46.5}V_{17}Fe_{3.5}$ alloy are shown in Fig. 2. After annealing, the peaks from the C14 Laves phase, which was the main phase of these alloys, were broad, and weak peaks from the second phase, which was identified as monoclinic α-ZrO_2, were found. After melt-spinning, the peaks from the main phase were stronger and sharper, and the peaks from α-ZrO_2 were also found. Fig. 3 shows SEM micrographs and EPMA mapping images of $Ti_{23}Zr_{10}Mn_{46.5}V_{17}Fe_{3.5}$ alloy. Many precipitates in the annealed sample were observed, as shown in Fig. 3a. Zr mapping image indicated that the segregation of zirconium occurred, which was attended with the Zr-rich precipitates (Fig. 3b), and moreover, oxygen concentrated in these precipitates. Furthermore, other precipitates were observed, which contained much more titanium. After melt-spinning, it was observed that the cross-sectional microstructure of a ribbon shaped sample had a chill zone on the under side, isotropic crystal grains and a few inclusions, as shown in Fig. 3c. Zr image mapping indicated that the inclusions contained much more zirconium (Fig. 3d) and that oxygen concentrated in these inclusions. However, the segregation, which was observed in the annealed sample, was hardly there.

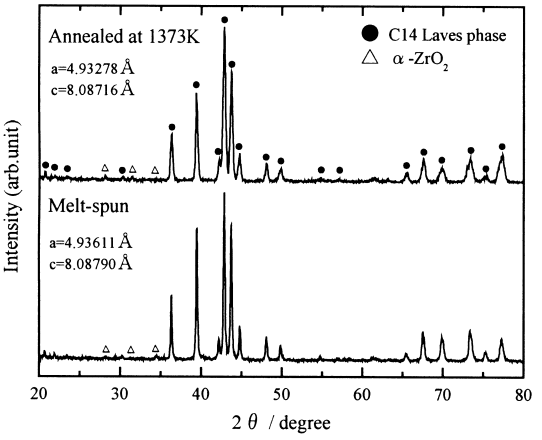

Fig. 2. X-ray diffraction patterns of the $Ti_{23}Zr_{10}Mn_{46.5}V_{17}Fe_{3.5}$ alloy.

3.2. $Ti_{35}Mn_{47}V_{15}Fe_3$ alloy

Fig. 4 shows the *P–C* isotherms of the $Ti_{35}Mn_{47}V_{15}Fe_3$ alloy, which was used for refrigeration output. After

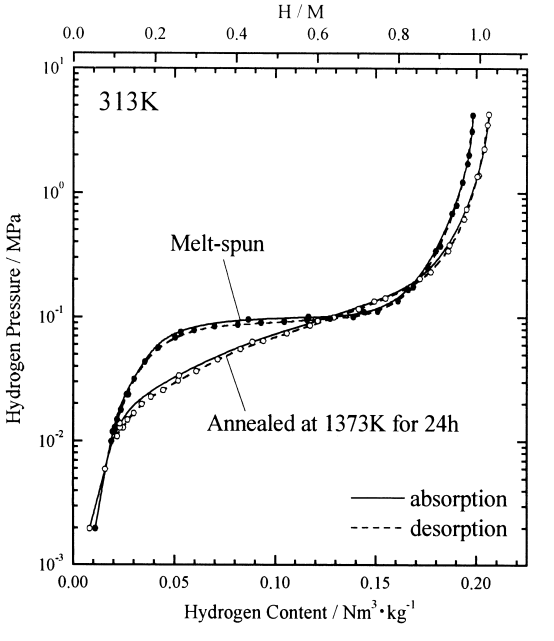

Fig. 1. *P–C* isotherms of the $Ti_{23}Zr_{10}Mn_{46.5}V_{17}Fe_{3.5}$ alloy.

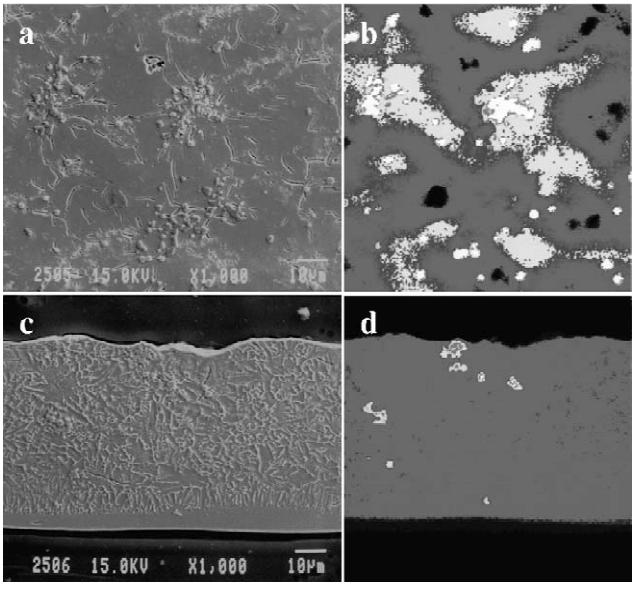

Fig. 3. SEM micrographs and EPMA mapping images of the $Ti_{23}Zr_{10}Mn_{46.5}V_{17}Fe_{3.5}$ alloy; (a) SEM micrograph and (b) Zr mapping image after annealing at 1373 K for 24 h, (c) SEM micrograph and (d) Zr mapping image after melt-spinning.

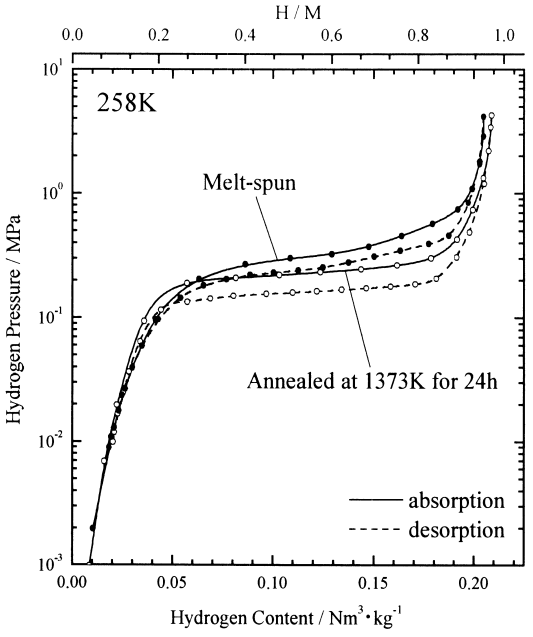

Fig. 4. *P–C* isotherms of the $Ti_{35}Mn_{47}V_{15}Fe_3$ alloy.

annealing, the *P–C* isotherms had comparatively flat plateaus. After melt-spinning, the plateau slopes did not become flatter than those of the annealed sample. Fig. 5 shows XRD patterns of the $Ti_{35}Mn_{47}V_{15}Fe_3$ alloy. After annealing, the peaks from the main phase were comparatively strong and sharp, and the weak peaks from the second phase, which was identified as an $E9_3$ structure (the space group is No. 227—*Fd3m*), were clearly observed. After melt-spinning, the peaks from the main phase were broader than the ones of annealed sample, and the peaks from the $E9_3$ structure phase became weaker. Fig. 6 shows SEM micrographs and EPMA mapping images of the $Ti_{35}Mn_{47}V_{15}Fe_3$ alloy. In the annealed sample, many precipitates were observed, which had dendritic morphology, as shown in Fig. 6a. The Ti mapping image indicated that the precipitates contained much more titanium (Fig. 6b), and moreover, oxygen concentrated in these precipitates. After melt-spinning, it was observed that the cross-sectional microstructure had a chill zone, isotropic crystal grains and a few inclusions, as shown in Fig. 6c. Ti mapping image indicated that the inclusions contained much more titanium (Fig. 6d), and moreover, oxygen concentrated in these inclusions. However, the Ti-rich dendritic precipitates, which were observed in the annealed sample, could not be clearly observed.

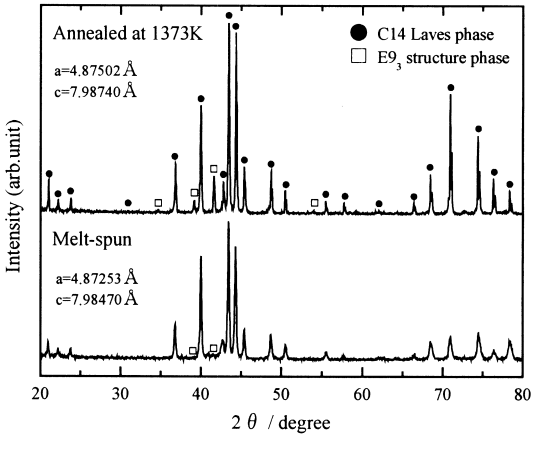

Fig. 5. X-ray diffraction patterns of the $Ti_{35}Mn_{47}V_{15}Fe_3$ alloy.

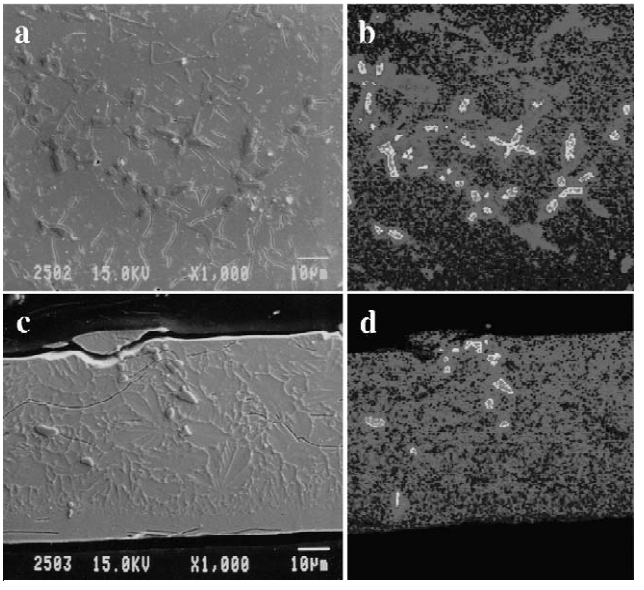

Fig. 6. SEM micrographs and EPMA mapping images of the $Ti_{35}Mn_{47}V_{15}Fe_3$ alloy; (a) SEM micrograph and (b) Ti mapping image after annealing at 1373 K for 24 h, (c) SEM micrograph and (d) Ti mapping image after melt-spinning.

3.3. TEM observation and EDS analysis

Fig. 7 shows TEM micrographs and EDS spectra of melt-spun samples of the $Ti_{23}Zr_{10}Mn_{46.5}V_{17}Fe_{3.5}$ alloy and the $Ti_{35}Mn_{47}V_{15}Fe_3$ alloy.

In the case of the $Ti_{23}Zr_{10}Mn_{46.5}V_{17}Fe_{3.5}$ alloy, Zr-rich and Ti-rich precipitates were observed in the annealed sample. Zr-rich precipitates, which were identified as α-ZrO_2, contained a large amount of oxygen. Ti-rich precipitates were also identified as the $E9_3$ structure phase. After melt-spinning, finer precipitates were observed (Fig. 7a). The EDS analysis revealed that these precipitates were Zr- and Ti-rich phases. The Zr-rich phase was more pronounced than the Ti-rich phase. Fig. 7b–d shows typical EDS spectra of the main phase, the Ti-rich phase and the Zr-rich phase, respectively. The Zr-rich phase was also identified as α-ZrO_2 and the Ti-rich phase was also identified as an $E9_3$ structure phase. Furthermore, a small amount of aluminum and silicon, which were inevitable impurities of ferrovanadium, were detected in the main phase, the $E9_3$ structure phase and α-ZrO_2. Silicon especially concentrated in α-ZrO_2. It was supposed that the segregation of zirconium affected the plateau property. It

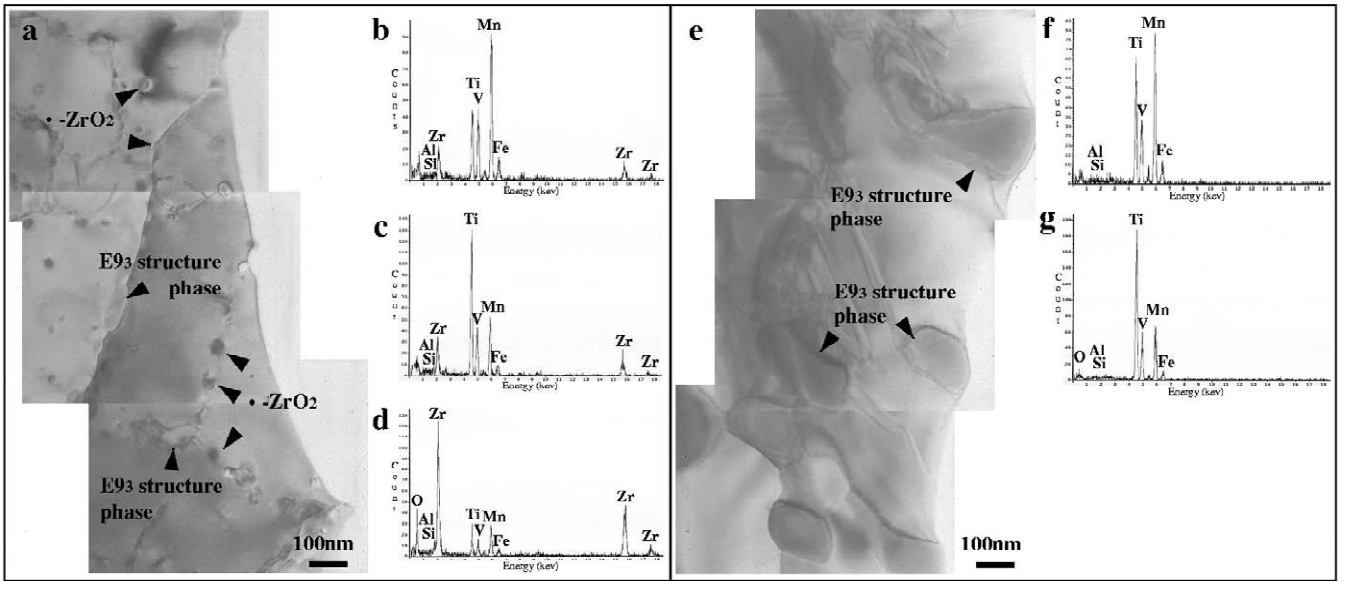

Fig. 7. TEM micrographs and EDS spectra of the melt-spun samples; (a) TEM micrograph, (b) typical EDS spectra of the C14 Laves phase, (c) typical EDS spectra of the $E9_3$ structure phase and (d) typical EDS spectra of α-ZrO_2 in the $Ti_{23}Zr_{10}Mn_{46.5}V_{17}Fe_{3.5}$ alloy. (e) TEM micrograph, (f) typical EDS spectra of the C14 Laves phase and (g) typical EDS spectra of the $E9_3$ structure phase in the $Ti_{35}Mn_{47}V_{15}Fe_3$ alloy.

was difficult to homogenize completely by annealing, because the diffusion rate of zirconium was much lower. After melt-spinning, the composition of the main phase was homogenized and a much finer α-ZrO_2 dispersed. As a result, the precipitation of the $E9_3$ structure phase, which had advanced when the phase contained oxygen, was prevented, so the crystallinity of the main phase improved.

In the case of the $Ti_{35}Mn_{47}V_{15}Fe_3$ alloy, Ti-rich precipitates were observed in the annealed sample. These precipitates, which were identified as an $E9_3$ structure, contained a small amount of oxygen. After melt-spinning, finer precipitates were widely observed (Fig. 7e). Fig. 7f and g shows typical EDS spectra of the main phase and these precipitates, respectively. These precipitates, which were also identified as an $E9_3$ structure, contained a large amount of titanium and a small amount of oxygen. Furthermore, a small amount of aluminum and silicon was detected in the main phase and the $E9_3$ structure phase. It was supposed that the morphology of Ti-concentrated region, which formed in process of solidification, affected the plateau property. The main phase and the $E9_3$ structure phase coexisted in the Ti-concentrated region of the as-cast sample. After annealing, the compositional homogeneity and crystallinity of the main phase were improved, so the plateau slopes became flatter. On the contrary, after being melt-spun, the interface between the main phase and the $E9_3$ structure phase widened, so the lattice strain between the two phases lowered the crystallinity of the main phase.

In the manufacture of Ti–Zr–Mn–V-based alloys, compositional homogenization and lowering the oxygen were desirable. Furthermore, lowered oxygen prevented oxide formation and increased the number of hydrogen storage sites.

4. Conclusion

In this present work, detailed observation of both Ti–Zr–Mn–V–Fe and Ti–Mn–V–Fe alloys was carried out. It was revealed that the segregation of zirconium in the $Ti_{23}Zr_{10}Mn_{46.5}V_{17}Fe_{3.5}$ alloy and the precipitation of the $E9_3$ structure phase in the $Ti_{35}Mn_{47}V_{15}Fe_3$ alloy affected their hydriding properties. The flatter plateaus were obtained by melt-spun $Ti_{23}Zr_{10}Mn_{46.5}V_{17}Fe_{3.5}$ alloy in spite of the presence of α-ZrO_2 because these α-ZrO_2 were much finer and dispersed homogeneously, and moreover, the composition of the main phase was homogenized. Therefore, compositional homogenization and lowered oxygen seem to be especially desirable in order to improve the performance of these alloys.

References

[1] T. Gamo et al., Int. J. Hydrogen Energy 10 (1985) 39–47.
[2] Y. Moriwaki et al., J. Less-Common Met. 172–174 (1991) 1028–1035.
[3] J.-L. Bobet et al., Int. J. Hydrogen Energy 25 (2000) 767–772.
[4] Y. Shudo et al., in: S. Hanada et al. (Eds.), The Fourth Pacific Rim International Conference on Advanced Materials and Processing, 2001, pp. 517–520.